Emergent remote stress-focusing drive submucosal collagen-fiber remodeling in intestinal anastomotic surgery

Brian P. Fleischer[a.,1.], Nhung Nguyen[a.,1.], Anshuman Pal[b.,1.], Kameel Khabaz[a.], Alkiviadis Tsamis[c.], Efi Efrati[d.], Thomas Witten[b.], John C. Alverdy[a.], and Luka Pocivavsek[a.,2.]

[a.] Department of Surgery, The University of Chicago, Chicago, IL, USA; [b.] Department of Physics, The University of Chicago, Chicago, IL, USA; [c.] Department of Mechanical Engineering, University of Western Macedonia, Greece; [d.] Department of Physics of Complex Systems, Weizmann Institute of Science, Israel

Following resection of a diseased segment of intestine, a reconnection (anastomotic) geometry is chosen to reduce postoperative stress and optimize outcomes. As proper healing of an intestinal anastomosis is strongly affected by its mechanobiology, much attention has been devoted to the conical-structures formed along the suture-lines, where stress-focussing is expected. However, geometric considerations reveal that in addition to the obvious loci of stress-focusing, additional remote locations of stress-focusing may form. We identify conical-structures that inevitably form within regions of otherwise uninterrupted tissue. In this work we use geometric-analysis, finite-element-modeling, and in-vivo experiments to investigate these emergent stress-focusing structures, their mechanical stresses, and the resulting submucosal collagen-fiber re-orientation, as these naturally arise in the side-to-side small-bowel anastomosis (SBA), the most common configuration performed in patients. Finite element modeling (FEM) predicts the appearance of remote high-stress regions. Allowing for tissue-remodeling, our simulations also predict increased dispersion of submucosal collagen fibers in these regions. In-vivo experiments performed on ten-week-old male C57BL/6 mice assigned the creation of side-to-side SBA or sham-laparotomy corroborate this result. Anastomoses were analyzed at sacrifice on post-operative day (POD) 14 and 88 with histologic-sectioning, staining, high-magnification-imaging, and submucosal collagen-fiber-orientation (κ) mapping. The mean and variance of κ, a measure of fiber dispersion, at POD-14 far from the anastomosis show similar values to those obtained for sham-operated mice, while the FEM-predicted loci of stress-focusing display statistically significant higher values. The values at POD-88 at all loci show no statistically-significant difference, and agree with those of the sham-operated mice at POD-14.

e-cone | d-cone | anastomosis |collagen fiber remodeling | stress focusing

DRAFT

Introduction

Surgery on the gastrointestinal (GI) tract generally involves removal (resection) of a diseased segment (cancer, inflammation) and its reconnection (i.e, an anastomosis) to reestablish continuity. The Achilles heel of this procedure involves unanticipated complications with healing such as tissues separation leading to leakage of toxic intestinal contents to over-healing with resultant strictures and occlusions of the newly formed connection. In intestinal surgery, multiple anastomotic geometries are routinely performed including end-to-end, end-to-side and side-to-side, with side-to-side being the most common (Fig 1). These anastomoses can be configured in a peristaltic versus non-peristaltic manner. Despite the general clinical success of these procedures, the science and soft-tissue mechanics involved are only superficially understood. Different techniques for bowel anastomosis have been developed and debated (1) since the days of Halsted (2). The surgical canon is filed with discussions invoking geometry and mechanics, though largely from a phenomenological standpoint (1–3).

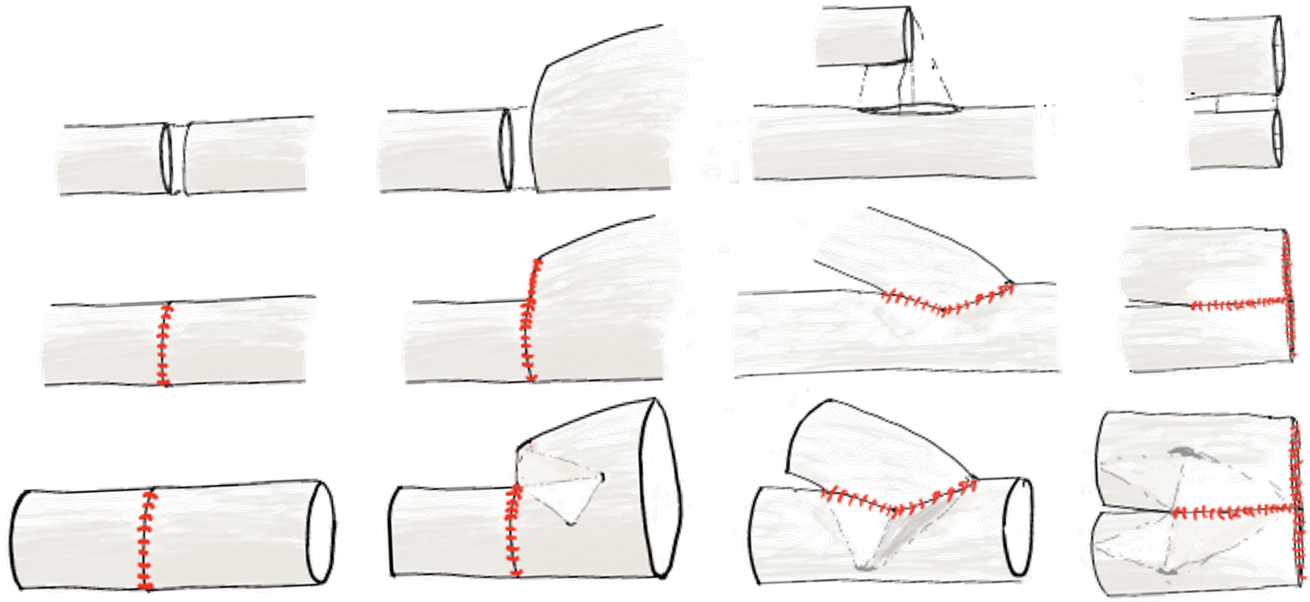

Fig. 1. Illustrations of common anastomosis geometries. (a) End-to-End. This anastomosis geometry possibly best mimics the preoperative geometry, yet it is limited to similarly sized limbs and typically requires manual suturing. (b) Billroth I; size mismatched end to end. Here the diameter discrepancy between the two limbs is absorbed by a sutured fold. (c) End-to-side. (d) Side-to-side. Thin (grey) arrows denote the loci of conical geometries where stress focusing is anticipated. Bold (blue) arrows point to regions of emergent remote stress focusing.

Surgeons can in large part manipulate the geometry of their anastomosis, guided by two fundamental phenomenologically-derived surgical principles: maintain tissue integrity and strive for a 'tension-free' suture line (4, 5). The former confines any viable anastomotic geometry to a class of tissue preserving shapes; meaning any combination of cutting and stitching is allowed however removal of tissue such as beveling beyond disease margins is often not. The latter imposes an even stronger condition on the suture line: length preservation or isometry; suture lines are not to be stretched. The field of intestinal surgery suffers from a fundamental lack of understanding

Significance Statement

Side-to-side anastomosis is the most commonly used geometry for bowel anastomosis, and is generally believed to be the least stressed anastomosis of diamater-mismatched tubular limbs. Geometric considerations and finite element modeling reveal that when the anastomosed tissue is pressurized from its closed rest state to allow for content flow, stress-focusing conical-structures arise in otherwise uninterrupted tissue, away from the suture line. In-vivo study using mouse model reveal significant collagen-fiber remodeling in these stress focusing locations. These results guide....

B.F. and J.A. performed animal experiments; B.F., K.K., L.P. and A.T. performed collagen fiber orientation analysis; B.F., L.P., A.P. and N.N. performed finite element analysis; A.P., L.P., and T.W. performed geometric analysis; B.F., N.N., A.P., T.W., J.A., and L.P. wrote paper.

No conflicts of interest.

[1]B.F. , N.N , and A.P. contributed equally to this work.

[2]To whom correspondence should be addressed. E-mail: lpocivavsek@bsd.uchicago.edu

of the geometry and mechanics underlying these experientially derived principles. Moreover, the postoperative geometry is often hidden behind non-stress bearing tissue layers, and assumes its true normal functioning form only under internal pressure and content flow. Advanced surgical devices such a staplers and robots have been engineered using empirical principles without a proper scientific basis. Commonly performed operations and hence complications (leaks, strictures, etc) still occur even when performed by expertly trained high volume surgeons operating in the most prestigious institutions. Therefore an in-depth analysis of intestinal anastomotic construction is needed beyond those that have traditionally been ascribed to be causative to complications (ischemia, tension, technique) despite the lack of evidence.

From a geometric standpoint, the gastrointestinal tract is a long curvilinear cylindrical shell (6). Resection of an intestinal segment leaves the surgical problem of reestablishing continuity by forming an anastomosis, which amounts to bringing two cylinders together following the above-mentioned established principals. As the thickness of the load-bearing tissue (sub-mucosal collagen layer) in bowel is much smaller than the typical bowel diameter, its mechanical response follows that of thin shells. Thin shells bend more easily than they stretch (7, 8), and easily buckle under in plane compressive loads (8). Mechanically modeling the intestine as a thin cylindrical shell that easily buckles was successfully used to predict the typical gut looping morphogenesis observed across many species (6). Pure bending deformations with zero in-plane stretching are termed isometries. However, such isometries are not always possible; in lieu of an available isometry the equilibrium configuration will balance the bending and stretching energy contributions. In some cases the optimal compromise between the stretching and bending deformations results in geometrically singular conical structures that focus stress (7, 8).

Singular conical structures in otherwise flat surfaces can be classified using a geometric charge called the integrated Gaussian curvature (which in the case of singular structures resides at a single point). There are several distinct ways to define the Gaussian curvature (), yet in what follows we only need to consider the special case of point-like Gaussian curvature in otherwise flat (Euclidian) surfaces. In this case, we can identify the integrated Gaussian curvature with the normalized difference between the surface area of all the points whose distance from the singular point is r and the area of a flat circle of similar radius, $A_0 = \pi r^2$:

$$\Phi = \iint K dA = 2\pi \frac{A_0 - A(r)}{A_0}.$$

This formula can be intuitively interpreted as the angular opening of the wedge of material removed to form the singular structure. In cases where material is added rather than removed the wedge angle is negative, as is the integrated Gaussian curvature. See Fig 2a and appendix A for more details.

Singular conical structures associated with a positive charge ($\Phi > 0$) are formed by removing a wedge of material and are called regular cones. In the surgical community these are often termed dog-ears. Singular conical structures with negative charge ($\Phi < 0$) are called e-cones (where 'e' stands for excess material), and form saddle like structures. Conical singularities with vanishing charge ($\Phi = 0$) are termed d-cones (where 'd' stands for developable, i.e. made from a flat sheet) (**?**). Figure 2(b) shows three points in side-to-side anastomosis associated with positive, negative and vanishing values of Φ.

Prior work from our group explored the geometry of a simple transverse closure or the Heineke-Mikulicz strictureplasty, where the doubling of peri-anastomotic luminal bowel diameter is linked to the isometric deformation of the anti-mesenteric bowel wall (9). While the strictureplasty shape

DRAFT

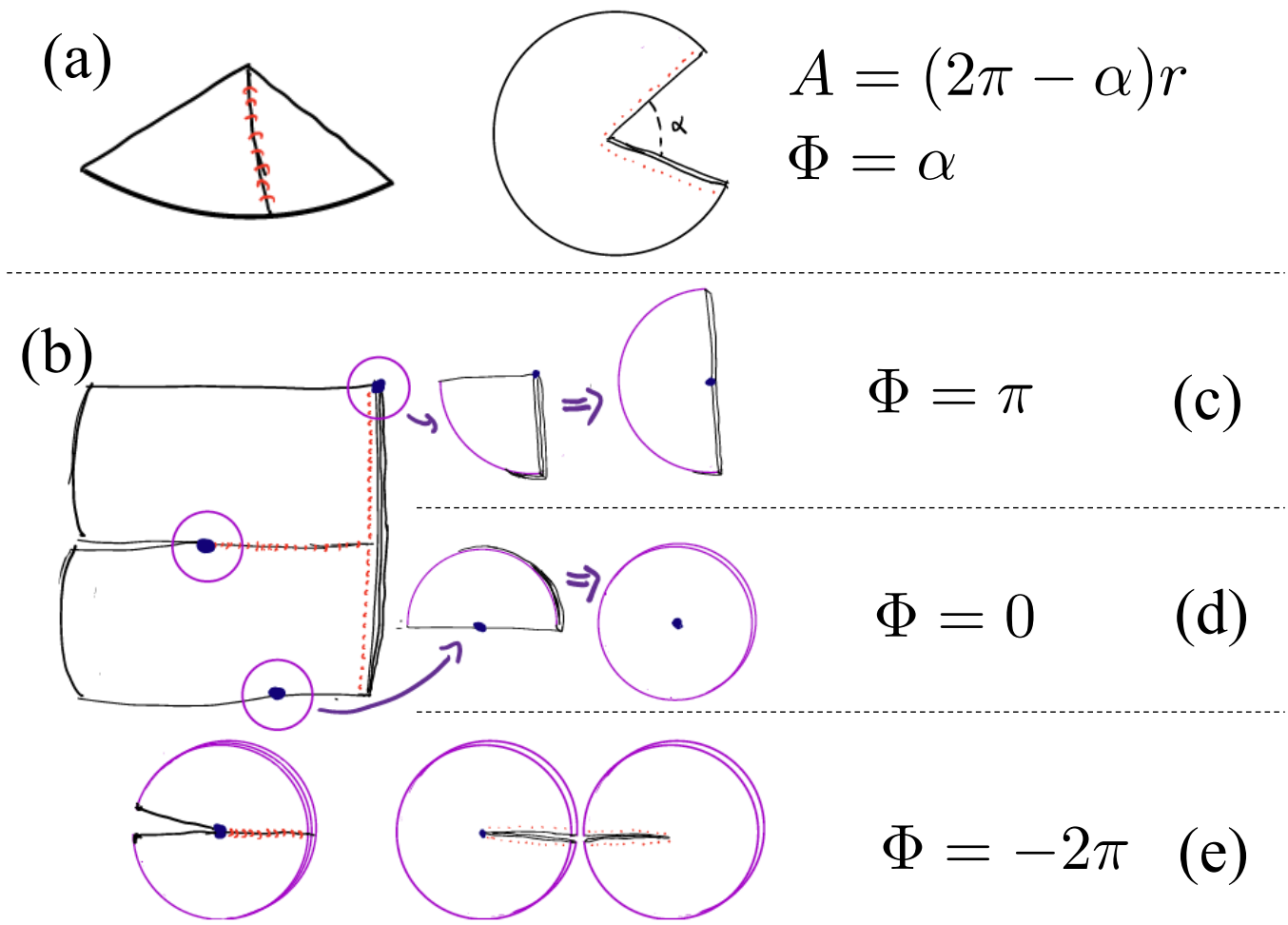

Fig. 2. The geometry of conical points and. (a)

displays regular cones, d-cones and an e-cone (see appendix figure 1) we showed that the resulting luminal geometry is dominated by the e-cone created at the middle of the suture line and the inevitable deformation it is associated with (10, 11). The locus of the e-cone formed in the Billroth I surgery is often called the "angle of sorrow" and is believed to focus stress and consequently be the source of postoperative leaks (). Such e-cones and regular cones are common for tissue sparing procedures as tissue preservation prevents the beveling of anastomosed limbs to match their geometry along the suture-line.

In 1887, the great American surgeon Dr. William Halsted revolutionized gastrointestinal surgery through his discovery that the collagen-rich submucosa is the load-bearing layer of the intestinal wall (2). Previous work from our group has elucidated the critical role that submucosal collagen fibers play in anastomotic healing (12–14); breakdown of these fibers leads to anastomotic leak. In fiber-reinforced composites, fiber orientation plays a strong role in setting the global and local mechanics of the system (15, 16). Bowel is living matter endowed with the capacity to locally change tissue structure in response to stimuli. While many strong perturbations such as local injury, ischemia, and exposure to collagenolytic bacteria overwhelm the tissue's ability to respond and cause sub-mucosal collagen breakdown (12, 14), we hypothesize that "softer-modes" of collagen remodeling arise in peri-anastomotic regions with non-native stresses.

The e-cones and regular-cones formed in these surgical procedures receive much attention (**?**) and are often closely examined mechanically after their creation. Surgeons appreciate that these anastomotic singular points can be sources of stress focusing; these regions are often reinforced with additional sutures, e.g. the often discussed 'anti-obstruction stitch' in side-to-side anastomosis or the purse-string suture placed at the angle of sorrow or 'Coffin Corner'. However, as is evident in panels b,c and d of figure 1 when an e-cone in created in cylindrical tissue, remote singular structures located away from the suture line and associated with no geometric charge (i.e. d-cones) naturally appear on the opposite side. The tissue reduction or addition that is associated with the creation of regular cones and e-cones along the suture line results in macroscopic tissue reorientation. The remote d-cones appear in order to reconcile this reorientation with the underlying cylindrical geometry. In many instances the unpressurized anastomosed tissue will show no evidence of these remote stress focusing structures. However, the collapsed lumen in this relaxed state cannot allow for content flow, necessary for normal function. Once pressurized to allow for content flow, the limbs adopt their cylindrical form away from the suture-line and the remote d-cones appear.

In this work we investigate the interaction between intestinal anastomotic geometry, mechanical stress, and collagen fiber distribution and remodeling in side-to-side small bowel anastomosis. We first establish, through finite element modeling, the appearance of d-cone type singular structures away from the suture line under pressurization of side-to-side anastomosis. We prove that the obtained d-cones are qualitatively and quantitatively crumpling-like structures akin to d-cones obtained and studied in less constrained environments (7**?** , 8). Numerically coupling the focussed stresses to tissue remodeling results in increased dispersion of submucosal collagen fibers in the vicinity of the formed d-cones. We subsequently design and perform the first ever clinically comparable side-to-side small bowel anastomosis mouse model and show that submucosal collagen away from the suture-line remodels only in regions that correspond to the location of d-cones in our geometric and finite element analysis.

DRAFT

1. Results and Discussion

A. Anastomotic Geometry. We simulate the bowel wall using a single layer Ogden-Gasser-Holzapfel (OGH) model, with the material properties adopted from previous work on intestinal mechanics (15). For simplicity and efficiency, we model only one of the limbs of the anastomosis and focus on the formed e-cone region and the cylindrical portion leading to it. Further details of material properties and boundary conditions are provided in the Methods section.

When a side-to-side anastomosis is newly created it is not spontaneously open, but remains in a closed configuration, with the longitudinal section in each of the limbs remaining straight and shut. This is especially true when the anastomosis is stapled and adjacent walls are forced to remain tangent to one another. For a functional anastomosis, the intra-luminal pressure within the GI tract provides the needed force to open the anastomosis. When a similar luminal pressure is applied to the simulated anastomosis it opens, and FEM simulations show the existences of locations that exhibit geometric focusing and high stress. Figure 3 shows a representative deformed geometry of one limb under pressure and the common channel open to its maximum extent with diameter d_{max}.

Figure 3 outlines the basic geometric structure of a maximally open anastomosis using the deformed shape from our simulation. As the pressure is increased the suture lines separate increasing the geometric charge of the associated e-cone and with it the maximal distance between the suture-lines ℓ. The formation of an e-cone to accommodate increase in lumen cross section is not unique to this geometry. HM stricture-plasty (see supplemental figure 1), size-mismatched end-to-end (Billroth I) and the end-to-side anastomosis all include an e-cone along their main suture line (supplemental

figure 2 - with FEA of CT derived rubber models). However, in the Billroth-I as well as in the side-to-side anastomosis, the un-pressurized anastomosed tissue may assume a flat, folded relaxed state that does not show the induced d-cones. The normals to the tissue on each of the sides of the flat folded configuration are all approximately parallel. In circular cylinders, the normal are parallel only along straight lines that are oriented along the cylinder's axis. Along the circumferential direction, the normals vary and complete a full turn around the cylinder. In particular, at any given point on a cylinder the normals vary only along one direction. In contrast, for a regular cone or an e-cone all rulings meet at a single vertex (at which the normal is not defined). (I think we need a figure to explain this or show it, the discussion of normal orientations starts to be hard to follow. We present the Gaussian curvatures in Figure 3- could we simply draw some normals onto this surface (see my attempt at this)?) If we now form an e-cone on the side of a cylinder, there are regions in the vicinity of the e-cone where the normals vary also along the long axis of the cylinder. Rulings in smooth developable surfaces can never cross and only meet at singular vertices. Upon pressurization of the anastomosis the effective e-cone opens and the limbs assume their cylindrical form far away from the suture. Consequently, there is a mismatch in local tissue orientation variation, which is reconciled by the formation of the d-cones.

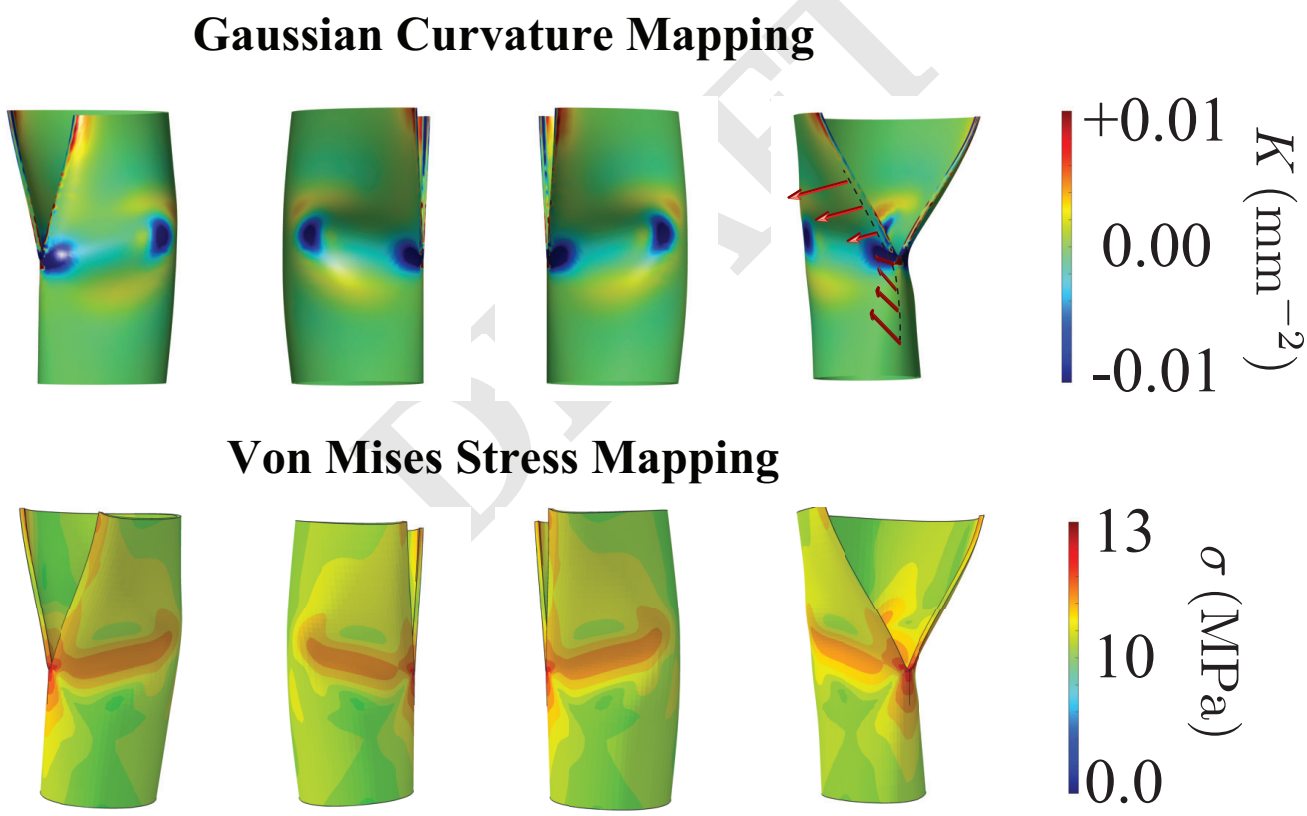

Fig. 3. Representative maximally deformed geometries of the open side-to-side anastomosis as simulated with finite elements. The principal curvatures are calculated at each point on the surface; Gaussian curvature, $K = \kappa_1 \cdot \kappa_2$, is mapped onto the surface showing that the majority of the deformed geometry is isometric to the undeformed cylinder, $K = 0$. Two regions of non-zero K exists: one on the suture line and two along a transitional region between the common channel and the limb (see figure 3 for geometric analysis). Bottom row shows the same deformed geometry with the stress field mapped onto the surface. Of note, the stress is nearly zero in all regions which deformed isometrically. However, the stress is three orders of magnitude above the baseline stress in regions corresponding to non-zero K; this indicates that the observed stress focusing is strongly linked to the underlying geometry.

The mechanics of thin elastic sheets is highly non-linear, and in order to provide intuition it is common to analyze the 'idealized' infinitely thin sheet. Such sheets fully display no in-plane strains; such conformation are called isometries. At the vicinity of the vertex of a conical structure in such

infinitely thin (isometric) sheets the normal curvatures may become arbitrarily large. Physical tissue, naturally, is associated with a finite thickness which regularizes this attempted divergence, by compromising the underlying geometry and introducing in plane strains. The diverging curvature along sharp creases that connect two conical structures are also similarly regularized. Geometrically, the in-plane deformations may give rise to Gaussian curvature, which typically vanishes for cylindrical surfaces. Mechanically, we expect these regions experience significant in-plane stress, that could eventually affect tissue remodeling. Figure 3 depicts the emergence of Gaussian curvature and the stress focusing in the vicinity of the conical structures and along the ridges connecting them. The stress values shown are for a simulation performed using the OGH material model, which has biological relevance and is used later in this paper to study fiber remodeling.

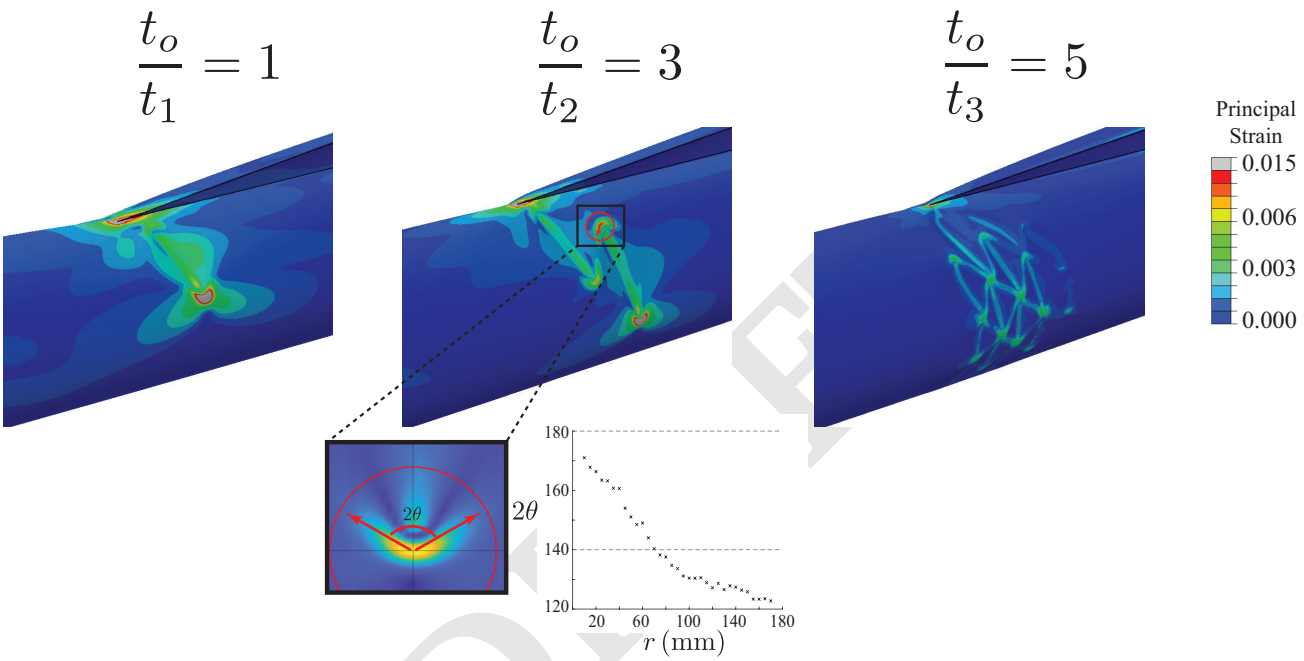

Fig. 4. Three side-to-side deformed geometries with anastomosis open generating a vertex e-cone in cylinders of varying thickness: $t_1/t_2 = 3$ and $t_1/t_3 = 5$ are shown. To quantitatively study the far-field mechanical and geometric consequences of the e-cone, we employ a simplified homogenous elastic material model in these simulations. In all three cases, all of the strain is again concentrated in the region of the transitional geometry as shown in figure 2, where the biologically relevant non-linear fiber-reinforced OGH material model is used. In all three cases, the e-cone vertex carries a large degree of tensile strain in a similar distribution. Interestingly, the far-field high-strain structures evolve in a cascading self-similar pattern with the thickest cylinder having a single crescent-like focus of high strain which bifurcates into two daughter centers which again bifurcate leading to a pattern qualitatively very reminiscent of crumpling. In crumpling, centers of high strain driven by non-isometric deformation called d-cones are connected by weaker strain-focused lines termed stretching ridges or the Witten ridge (7).

To more systematically study the stress distribution in this geometrically non-linear region, we performed simulations using a simpler Neo-Hooken material to be able to better compare with existing theories of conical singularities. Figure 4 shows the evolution of the stress pattern as a function of decreasing shell thickness; for the thickest shell, a singular center of high stress appears far-field from the e-cone and is connected by a ridge like region of higher than baseline stress. As the thickness decreases, the far-field structure bifurcates and develops the Yoshimura buckling pattern typical for longitudinally loaded cylindrical shells (17) consisting of crescent shaped singular points connected by elongated stressed regions. These are reminiscent of the well studied d-cone structures obtained by circular confined thin flat sheets, and Lobokovsky-Witten stretching ridges that connect conical points in thin flat sheets. Further analysis show that the similarities between these structures is not only qualitatively, but quantitative, see inset of figure 4 and Appendix A. This identification brings with it quantitative understanding of the mechanical in-plane stress structure in the anastomosed tissue. In particular, it allows to theoretically predict the loci of maximal stress,

and estimate its magnitude given the physiological values of the tissue thickness and anastomosis geometry. we should, and can, back this up by a back of the envelop calculation Some analysis here with a calculation would be useful, otherwise this section reads more as simply an observational section of the simulation results.

B. Tissue Response to a d-cone.

Biological Experiments. The suture line is known to be an area of tissue injury and remodeling. However our interest is the biological response to the induced d-cones and Witten ridges away from the suture line; as such a side-to-side anastomosis was performed in ten week-old male C57BL/6 mice who, following recovery were sacrificed on either post-operative day (POD) 14 or 88. Sham-operated mice (anesthesia, skin incision, and immediate closure) served as controls. In the experimental mice, anastomotic and peri-anastomotic tissues were harvested and sectioned at a pre-determined standardized depth. Images were then taken along the perimeter of the anastomosis away from the suture line every 0.2 mm, where tissue integrity was preserved such that Trichome staining allowed identification, visualization, and directional mapping of sub-mucosal collagen fibers as a function of distance from the anastomotic vertex. Quantification of collagen fiber orientations was performed by fitting the fiber angles from each image to a transversely isotropic and π-periodic von Mises distribution. The mean collagen angle was 30° as reported in the literature Brian needs to verify this, he does not have it in the methods. The spread of collagen angles per image is quantitated through the dispersion parameter κ (see Methods). κ varies between 0 and 1/3 and is used in many continuum fiber reinforced models to take into account variance in fiber angles. Tissues with perfectly aligned fibers have $\kappa = 0$, while tissue with no fiber orientation have $\kappa = 1/3$. Figure 5A shows the distribution of κ values obtained every 0.2 mm along a segment of normal bowel in the control laparotimized animals with a mean of 0.11. Figure 5B shows similar data obtained in experimental animals at POD 14. The aggregate distribution in this case becomes asymmetric with a shoulder appearing at higher κ values that was not present in the control group. This shoulder can be understood by separating the different 0.2 mm segments into two groups based upon our finite element simulations and the predicted location of d-cones. One group is images from tissue away from the anastomotic vertex and e-cone (red symmetric distribution in figure 5B), while the second group is tissue forming the perimeter around the vertex (blue symmetric distribution in figure 5B). The later distribution (near vertex) has a mean $\kappa = 0.13$ and is shifted to the right, while the former (far-field) has a mean of 0.11 similar to the control. Figure 5D shows that the far-field distribution is statistically identical to the controls, while the near vertex distribution is significantly different. When a similar analysis was performed on mice far from surgery at POD 88, no significant difference could be appreciated in the near-vertex and far-field groups, both being identical to the controls.

While intestinal tissue is best modeled in its native state as a fiber-reinforced composite with two primary fiber-families running in a helical pattern through the submucosa in the theta-z plane(15), we observe a shift in the distribution of the orientation of submucosal collagen fibers in the immediate post-operative period. As noted in our POD 14 population, there is a distinct and statistically significant difference in the orientation of the submucosal collage fibers when comparing those regions of bowel that experience standard stress fields with those that experience stress-focusing and d-cone deformation patterns, as informed by our simulations. This can likely be attributed to the biological tissue's desire to remodel in such a way so as to minimize the effects of these newly felt stress-focused fields. This shift in collagen fiber orientation leads the tissue away from its previous anisotropic response to stress to a more isotropic material, altering its deformation response to insults and likely its permanent function and appearance.

DRAFT

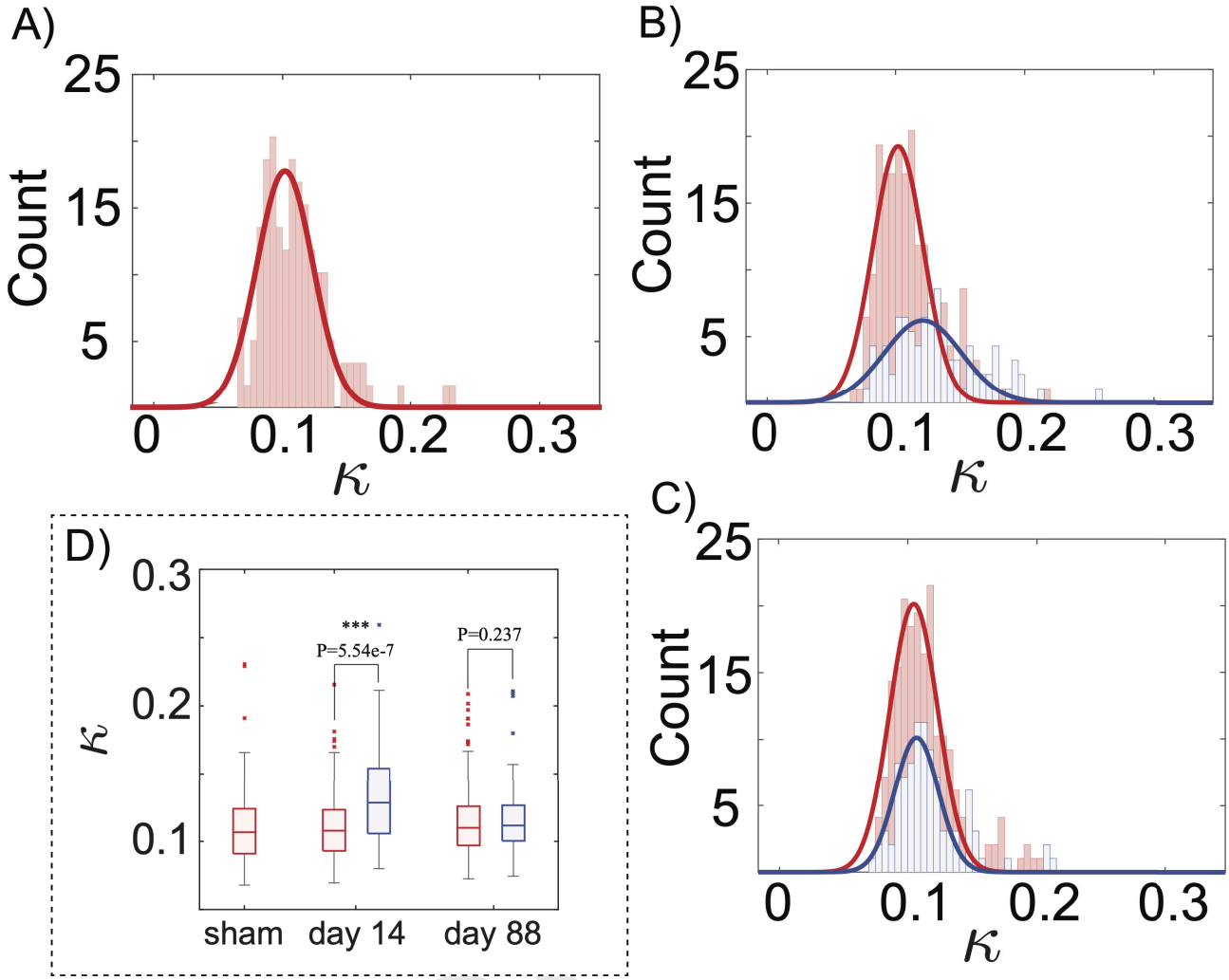

Fig. 5. Distribution of κ values through anastomosis as a function of location (red indicating regions of isometric geometry, blue indicating regions of geometric focusing) for A) Sham-operated mice as well as anastomoses harvested at B) POD 14 and C) POD 88. D) The regions of the anastomosis that experience isometric geometry have similar κ values regardless of post-operative time point, while there is a statistically significant difference at the noted geometric focusing location on POD 14 that reverts at POD 88.

However, as post-operative time progresses, we note a return to the native orientation of these collagen fibers in those regions of the anastomosis that previously experienced stress-focusing and d-cone deformation patterns. This can likely be attributed to the permanent morphologic changes we observe in these anastomoses as they become grossly dilated and often fecalized at long time points. This adaptation of the affected bowel geometry via dilation leads to a relaxation in the stress-focusing initially felt after imposition of the non-linear geometry on the system, leading to re-organization of the submucosal collagen fibers into a conformation closely resembling its initial state. The scope of this work extends far beyond the bounds of this specific anastomotic construction. We know that similar geometric aspects that lead to the formation of stress-focused points exist in other commonly used conformations as well. The strictureplasty, an operation performed to relieve narrowing of the lumen of the bowel, results similarly in the formation of e-cones through its efforts to longitudinally open and transversely close an incision through the anti-mesenteric surface of the bowel(9).

Submucosal collagen fiber remodeling model. The next focus of this study is to explore the mechanism driving changes in the dispersion of submucosal collagen fibers in the above experiments. To elucidate

this mechanism, we start the simulations with an aligned fiber state where the dispersion κ is set to zero and enrich the OGH model with a collagen fiber remodeling process induced by the stress focusing and loading state. The remodeling of the submucosal collagen fibers is triggered when the stress becomes larger than a critical value: $\sigma_{vs} > \sigma_{cr}$, where we use the Von-mises stress for an effective measure of the stress state (18). Within regions of collagen fiber remodeling, the fibers' orientations gradually tend to align with the principal loading directions (19). For uniaxial loading this implies an alignment with the loading direction and hence a reduction fiber orientation dispersion $\kappa \to 0$. In contrast, for equal biaxial loading where all directions are equivalent this leads to a more isotropically dispersed state where $\kappa \to 1/3$ (19). While such fiber reorientation models were applied to cardiovascular tissues, we present here the first integration of fiber remodeling with the OGH constitutive law the fibers give rise to, and carry out the first such implementation to bowel tissue.

It also explains our experimental observation of the localization of collagen fiber orientation dispersion to the stress focusing regions.

Specifically, for the elements that experience a stress that is above the threshold value σ_{cr}, the stretches λ_1, λ_2 along the principal circumferential and longitudinal directions are determined. These values provide the loading states that dictate the preferable dispersion value κ_p of the collagen fibers. Denote $g_i = \lambda_i - 1$, where $i = \overline{1,2}$. If $|g_1| * |g_2| > 0$, the element exhibits a biaxial stress state and therefore the preferable direction of the collagen fibers are determined as follows:
For $|g_1| > |g_2|$:

$$\kappa_p = \frac{1}{3}\frac{|g_2|}{|g_1|} \qquad [1]$$

For $|g_2| > |g_1|$:

$$\kappa_p = \frac{1}{3}\frac{|g_1|}{|g_2|} \qquad [2]$$

Note that if $|g_1| \gg |g_2|$, the element experiences a near uniaxial loading state. Hence, from Equation 4, the preferable value of κ_p becomes 0 as in the limit of uniaxial loading. In other words, the collagen fibers remodel toward the principal uniaxial loading direction, and thus exhibits a more aligned state. The same limit is obtained from Equation 5 if $|g_2| \gg |g_1|$. On the other hand, if $|g_1| = |g_2|$ then both Equation 4 and 5 gives the limit of an equal biaxial loading in which κ_p becomes 1/3. This means that collagen fibers becomes more dispersed and experience a more isotropic distribution. For any state of loading in between the preferable value of the dispersion can be obtained from Equations 4 and 5. Since we start with the assumption of $\kappa = 0$, the condition $|g_1| * |g_2| < 0$ that resembles a uniaxial loading state does not cause a change in the dispersion value: $\kappa_p = \kappa = 0$. However, future development of the computational model can include an improvement for this assumption where a more non-homogeneous initial dispersion state is assumed.

The remodeling happens to adjust the initial fiber dispersion of each element towards the targeted preferable direction dictated by the loading state as established above. A remodeling rate equation (19) is used to govern this adjustment process:

$$\frac{d\kappa}{dt} = \frac{1}{\tau}\left(\kappa_p - \kappa\right) \qquad [3]$$

where τ is the rate of the remodeling.

The above model is implemented using the user material subroutine VUMAT in Abaqus. Details of the subroutine implementation are provided in the Appendix. Our simulations are able to couple the

DRAFT

non-linear, complex loading situations of a pressurized side-to-side anastomosis with the evolution of the dispersion value updated based on the remodeling Equations 4-6. The rate of the remodeling is adjusted by varying τ, hence provides a capability to capture how fast or slow the remodeling happens in real experiments. Simulations with our developed model shows that the anastomosis opens and in the stress focusing regions the stress states are close to an equal biaxial stress state that drives the submucosal collagen fibers to experience a more dispersed state: $\kappa_p \to 1/3$. Figure 2 shows this increase of the κ value from the initial dispersion state. The distribution of the dispersion values from the numerical simulations at the end of the remodeling process is qualitatively consistent with the experimental measurement shown in Figure. we should consider shortening this section's footprint in the main text and move parts to the appendix.

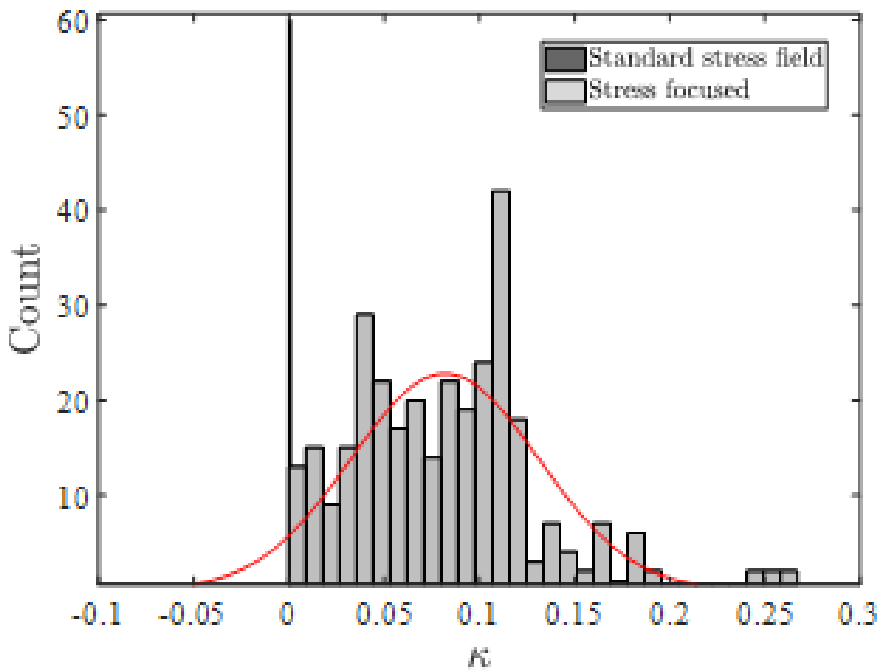

Fig. 6. FEM simulations with a collagen remodeling fiber shows the increase of dispersion value in the stress focused region.

While our prior work on stricture-plasty generated an e-cone on a cylinder, we did not systematically study the far-field effects away from the e-cone vertex (9, 11).

2. Conclusions

the entire conclusion section is guided by collagen remodeling. We should make it wider Since collagen fibers have been reported to have the capacity to remodel under applied stress (19), we investigated how stress is distributed along the amorphous non-linear configuration of a side-to-side anastomosis and its association with changes in collagen fibers. We developed both a novel operative technique to create a physiologically relevant small bowel side-to-side anastomosis as well as a new stress induced remodeling model coupled with OGH constitutive modeling incorporating criteria from previous experimental and numerical studies on collagen remodeling (19). Firstly, remodeling only occurs if the applied stress is greater than a set critical value. This finding is consistent with our experimental data where the changes in fiber dispersion are only observed in stress-focusing areas. Secondly, collagen fibers remodel in a manner in which the dispersion value depends on the loading states with two limits. If the loading state is equal biaxial, the collagen becomes more dispersed and

it becomes more aligned in the uniaxial loading state. Due to the first criterion, the collagen fibers only remodel in the stress focus regions, which is again demonstrated in our biological experiments. This explains why there are no changes in collagen dispersion in the non-stress-focused regions in our experimental data. The second criterion further predicts that the dispersion becomes higher, indicating a more dispersed fiber state in these areas. Furthermore, our model predicts that after remodeling occurs, the stress of the elements inside the remodeling area drop, alleviating the stress focusing effect that the bowel experiences.

Materials and Methods

***In Vivo* Model.** All mouse experiments were approved by the Institutional Animal Care and Use Committee (IACUC) of the University of Chicago (ACUP protocol 72417). Ten week-old male C57BL/6 mice (Charles River Laboratories©, Kingston, NY) were used for all experiments and were allowed unrestricted access to standard chow diet and tap water both pre- and post-operatively. All mouse experiments were run in duplicate.

All non-control or sham-operated mice were anesthetized and underwent laparotomy with handsewn small bowel anti-peristaltic side-to-side, functional end-to-end anastomosis using 8-0 monofilament, non-absorbable suture (Surgipro™ II Monofilament Polypropylene), following appropriate sterile technique. Laparotomy incision was closed in two layers using 3-0 braided, absorbable suture (Covidien Polysorb™). Anesthesia was obtained via intra-peritoneal injection of 100 mg/kg ketamine and 10 mg/kg xylazine(20). Post-operatively, all mice were resuscitated with 1mL sterile water injected subcutaneously. Intra-operatively, a segment of small bowel was identified and transected, with special attention paid to ensure there was no interruption of blood supply to the bowel. The two ends of the bowel were spatulated along the anti-mesenteric surface and the common channel of the anti-peristaltic side-to-side, functional end-to-end anastomosis was created. The common anastomotic channel length was approximately 2-3 times the diameter of the bowel lumen.

A. Tissue Harvesting and Histology. The mice were sacrificed on either POD 14 or 88. The previous laparotomy incision was re-opened and the underlying bowel was carefully dissected out. The anastomosis and peri-anastomotic tissues were harvested and pressurized with 100μL of formalin to ensure bowel was fixed in a non-collapsed conformation. All harvested tissue was then formalin fixed and embedded in paraffin to prepare for sectioning and staining.

Tissue samples were sliced into 5μm thick sections, which subsequently underwent Trichome staining. Sections were obtained at pre-determined depths, correlating with entry into the lumen of the bowel and areas of predicted stress-focusing as calculated using our computer simulations.

B. Sample Imaging. All sample imaging was performed at 100x/1.3NA oil 0.2mm WD magnification using a Zeiss Axioskop™ upright histology microscope. Images were captured around the perimeter of each sample at predetermined locations, approximately every 0.2mm of tissue.

C. Image Analysis. Initial image analysis was performed through Fiji and its Directionality plugin (v2.0). All captured microscopy images were cropped such that only the submucosal collagen fibers were included and rotated such that the horizon was set to 0°. The aforementioned program was then implemented to characterize the orientation of submucosal collagen fibers in each image via a Fourier Transformation. These results were confirmed using a separately validated image processing algorithm(21).

DRAFT

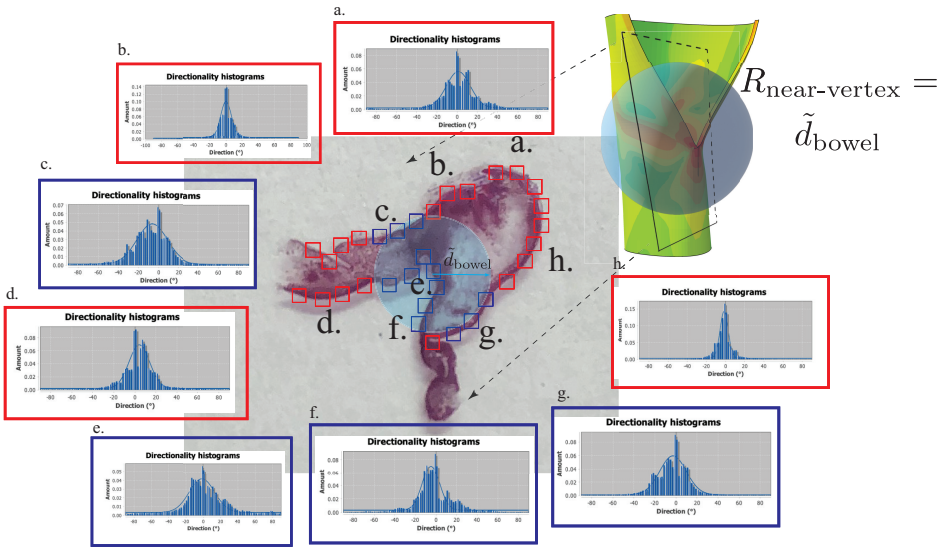

Fig. 7. FEM simulations with a collagen remodeling fiber shows the increase of dispersion value in the stress focused region.

D. Data Analysis. The collagen fibers of the small intestinal submucosa were assumed to consist of an interweaving lattice structure of two distinct fiber populations that run along the longitudinal axis of the bowel and intersect in a cross-ply fashion(15, 22). Further, it was assumed that the collagen fibers are distributed according to a transversely isotropic and π-periodic von Mises distribution, which is commonly assumed for directional data. We normalized the standard π-periodic von Mises distribution with the resulting distribution in Equation 7(23).

$$\rho(\theta) = 4\sqrt{\frac{b}{2\pi}}\frac{exp[b(cos(2\theta)+1)]}{erfi(\sqrt{2b})} \qquad [4]$$

Our raw data obtained via image analysis techniques previously described were plotted and fit to the above curve. After solving for the concentration parameter b in Equation 1, we solved for the structural parameter κ using Equation 8(16).

$$\kappa = \frac{1}{2} + \frac{1}{8b} - \frac{1}{4}\sqrt{\frac{2}{\pi b}}\frac{exp(2b)}{erfi(\sqrt{2b})} \qquad [5]$$

E. Statistical Analysis. Images obtained around the perimeter of each sample at predetermined locations were siloed into locations where we do not see stress-focusing in our simulations and those areas where we see geometric and stress focusing in our simulations. The κ values previously obtained for every image captured were then compared between these two silos using a one-tailed, two-sample unpaired t-test for samples of unequal variance.

F. Finite Element Modeling. A computational model for a side-to-side anastomosis was constructed in the commercial finite element (FE) software Abaqus (Dassault Systemes, RI) (24) as shown in Supplemental figure 1. Specifically, a slit was created on the wall of a cylinder to model the suture lines on the anti-mesenteric surface of the tubular bowel. In the finite element simulations, we model only one limb of the anastomosis, assuming symmetry with the second. This is done to decrease the computational cost of the simulation, since simulations with both limbs showed no appreciable differences compared to the single limb simulation (see supplemental video 1 and supplemental video

DRAFT

2). Boundary conditions along the suture line are used to reproduce the mechanical effect of the kinematic coupling that the sutures impose. Pressure due to the flow of the luminal contents inside the bowel was applied to the internal surface to drive the opening of the anastomosis. The main load bearing layer of the intestinal wall, the submucosa, is a fiber-reinforced layer with collagen distributed in the soft elastin matrix (15, 25, 26). To capture this structural aspect and the large deformation of the bowel tissue, the Ogden-Gasser-Holzapfel (OGH) model was utilized (15, 25, 26). We simulate the bowel wall as a single layer OGH model with the material properties adopted from previous work on intestinal mechanics (15): $\mu = 1.58$ kPa, $k_1 = 22.01$ kPa, $k_2 = 12.1$, and $\kappa = 0$. The mean collagen fiber direction in the submucosa layer is $\theta = 30^0$ as suggested in (15). The model is based on a strain-energy function $\Phi = \Phi_m + \Phi_f$ composed of contributions from the elastin matrix Φ_m and the collagen fibers Φ_{fi}. The specific forms for these energy functions are as follows:

$$\Phi_m = \frac{\mu}{2}\left(\bar{I}_1 - 3\right) + \frac{K}{2}\left(\frac{J^2-1}{2} - ln(J)\right) \quad [6]$$

$$\Phi_{fi} = \frac{k_1}{2k_2}\left[\exp\left(k_2\bar{E}_i^2\right) - 1\right] \quad [7]$$

$$\bar{E}_i = \kappa\left(\bar{I}_1 - 3\right) + (1-3\kappa)\left(\bar{I}_{4i} - 1\right) \quad [8]$$

where μ and K are the shear and bulk modulus of the elastin matrix, respectively, $J = det(F)$ represents the volume ratio between the deformed and undeformed tissue with F is the deformation gradient. To enforce a nearly incompressible behavior for the bowel material (15) where $J \to 1$, a high numerical value for the ratio K/μ was used. $\bar{I}_1 = J^{-2/3}I_1$ where $I_1 = tr(C)$ is the first invariant of the right Cauchy Green tensor $C = F^TF$ widely used to study the nonlinear elasticity of soft elastomeric materials and tissues (15, 25, 26). Two symmetric families of collagen fibers $i = 1, 2$ are assumed to orient along an angle $\pm\theta$ with respect to the circumferential direction, corresponding to two mean directions A^i (15). k_1 is the fiber stiffness, and k_2 is a dimensionless parameter correlating to the non-linearity of the collagen fiber's response. κ is the dispersion of the collagen fibers. $\kappa = 0$ corresponds to an aligned state of collagen fibers along the mean direction and $\kappa = 1/3$ corresponds to an isotropic dispersion state. $\bar{I}_{4i} = J^{-2/3}I_{4i}$ and $I_{4i} = A^i.CA^i$ gives the square of the stretch along the mean direction A^i of the ith fiber family.

DRAFT

3. Appendix

A. d-cone analysis. *Need Neo-Hookean parameters for the Geometry simulations.*

Our analysis is done at a fixed time step, far along into the simulation that we can safely assume a steady-state stress distribution has been attained. We import the (von Mises) stress data for the region of interest (i.e., the region around the cut tip) from Abaqus to Matlab using the package Abaqus2Matlab (**?**). This data is defined on the undeformed cylinder. For ease of viewing and subsequent analysis, we unroll and flatten the cylinder to a rectangle, using the standard mapping $(\theta, z) \mapsto (x, y)$, where θ is the azimuthal coordinate and z is the axial coordinate on the cylinder. Finally, using peak detection, we isolate the point singularity we wish to study, and keeping in mind the measurements to follow, also interpolate this isolated data over a fine grid (see supplemental figure 2A). We wish to measure quantities along the arc of the crescent singularity, i.e., as a function of the arc length coordinate s. In other words, we wish to extract a meaningful 1-dimensional data field, say $\sigma(s)$ for stress, from a 2-dimensional one, $\sigma(x, y)$. To do this, we draw circles of increasing radius r centered at the tip of the crescent (located using peak detection algorithms), and measure σ only along this circular contour. Here, the radius $r \approx s$, the desired arc length coordinate, since

the crescent is not sharply curved. This gives a polar distribution of the data along the circle (as a function of the angle ϕ), which has a tri-lobular structure, as expected (each lobe is a maximum or peak), see supplemental figure 2B. Since we are only interested in the crescent here, we only care about the two side peaks. Again, using peak detection, we find the angular locations of the three lobes. Shifting the central peak to the y-axis ($\phi = 0$), we can then measure the opening angle of the two side lobes, call them ϕ_1 and ϕ_2. Measurements show that $\phi_1 = -\phi_2 = \phi_{cresc}$. This gives us a value for that particular circle, of radius r. Doing this for a range of circles, we get the desired distribution $\phi_{cresc}(r) \approx \phi_{cresc}(s)$ along the arc of the crescent. The d-cone opening angle is $\Delta\theta = 2\phi_{cresc}$. Similarly, we can get the stress along the two arms of the crescent, $\sigma_1(s)$ and $\sigma_2(s)$. Measurements also show that $\sigma_1(s) \approx \sigma_2(s)$. The same analysis applies to the simple d-cone situation, with the just the initial data preparation being simpler since the undeformed geometry is already a rectangle, and not a cylinder.

B. ??. Figure 10 (appendix) shows our approach. Since there lacks a general theory of d-cones, we perform a comparison between the side-to-side geometry, where our hypothesis is that an e-cone drives the appearance of a remote d-cone, with a standard method of generating a simple d-cone in plane sheets, indentation of a sheet into a cylinder. Top panel in figure 10 shows the appearance of a simple d-cone as the elastic sheet evolves from a local stretching from indentation to global folding and local stress focusing as the d-cone evolves. Bottom panel in figure 10 shows the appearance and evolution of the remote high stress singularity in the side-to-side simulation. Given the boundary conditions and the loading there is no doubt that the planar indentation simulation is that of a d-cone. There is strong qualitative similarity between the appearance of the crescent-like strain distribution of the simple d-cone and the remote singularity in the cylinder. Figure 5 shows our data for the canonical d-cone opening angle 2θ plotted as a function of distance from the peak stress. The simplest theory of d-cones states that 2θ is constant at 140^0. why is the angle important (**?**), though this is only in the limit of linear elasticity and planar initial geometries. The nearly identical dependence of 2θ on radial distance for the two simulation, we believe, proves that the remote singularity being driven by the e-cone is indeed a d-cone.

DRAFT

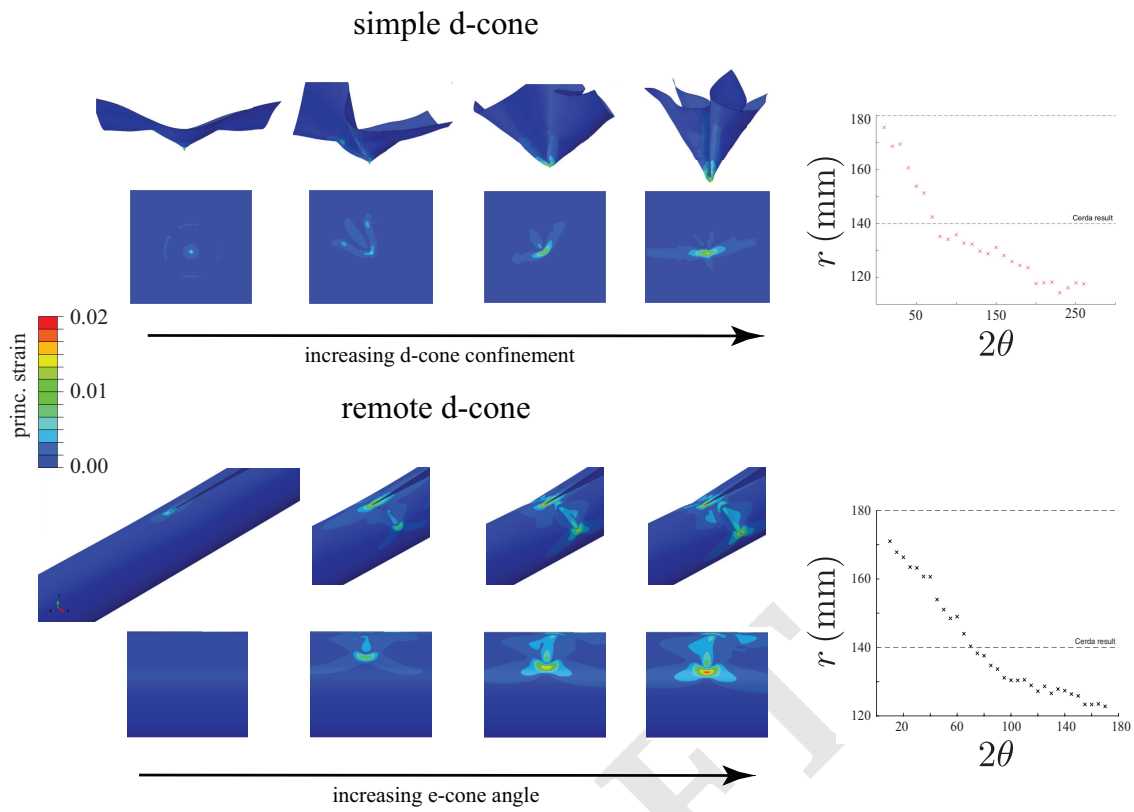

Fig. 8. The evolution of the far-field strain pattern with thickness (figure 4) qualitatively supports the hypothesis that this region of the cylinder deforms by forming d-cones locally. Given the lack of a general theory of d-cones, to prove that the remote singularity seen in our simulations is indeed a d-cone, we opted to compare the strain distribution of a simulated simple d-cone with the remote far-field d-cone. The simple d-cone is generated by indenting a flat membrane into a hollow cylindrical support, this is the classic loading geometry well known to generate a d-cone at the point of indentation (7**?**). We show both the deformed geometry and the projected strain distribution onto the undeformed initial shape. For the simple d-cone, the initial core region shows a symmetric strain distribution as expected for localized stretching due to indentation. Once the membrane undergoes a macroscopic bending/folding, the classic crescent-like distribution of strain at the d-cone core appears (**?**). With further confinement, the crescent distribution remains focused but evolves in its shape for an elastic systems such as simulated here. The bottom row shows the evolution of a single remote d-cone on the cylinder with increasing e-cone angle; the same crescent shape is observed in the strain distribution around the core. This data shows that the simple d-cone and the remote d-cone have qualitatively the same distribution of strain in the core region, allowing us to make the claim that the far-field high strain singularity in the cylinder is indeed a d-cone. The opening angle, 2θ, of the crescent-like strain distribution seen in d-cones is measured as a function of radial distance away from the peak core stress as outlined in figure 10. Note that the angle reaches an asymptotic limit once a given distance from the core itself. The simple d-cone shows a limiting $2\theta \sim 115^o$, while the remote d-cone has $2\theta \sim 125^o$. This proves quantitatively that the two structures are nearly identical and as such that the remote far-field strain focused singularity induced by the e-cone is a d-cone. Moreover, the opening angle falls into the theoretical range calculated for d-cones (**?**).

DRAFT

4. Supplemental Figures

SUUPLEMENTAL FIGUR 2B

ACKNOWLEDGMENTS. Please include your acknowledgments here, set in a single paragraph. Please do not include any acknowledgments in the Supporting Information, or anywhere else in the manuscript.

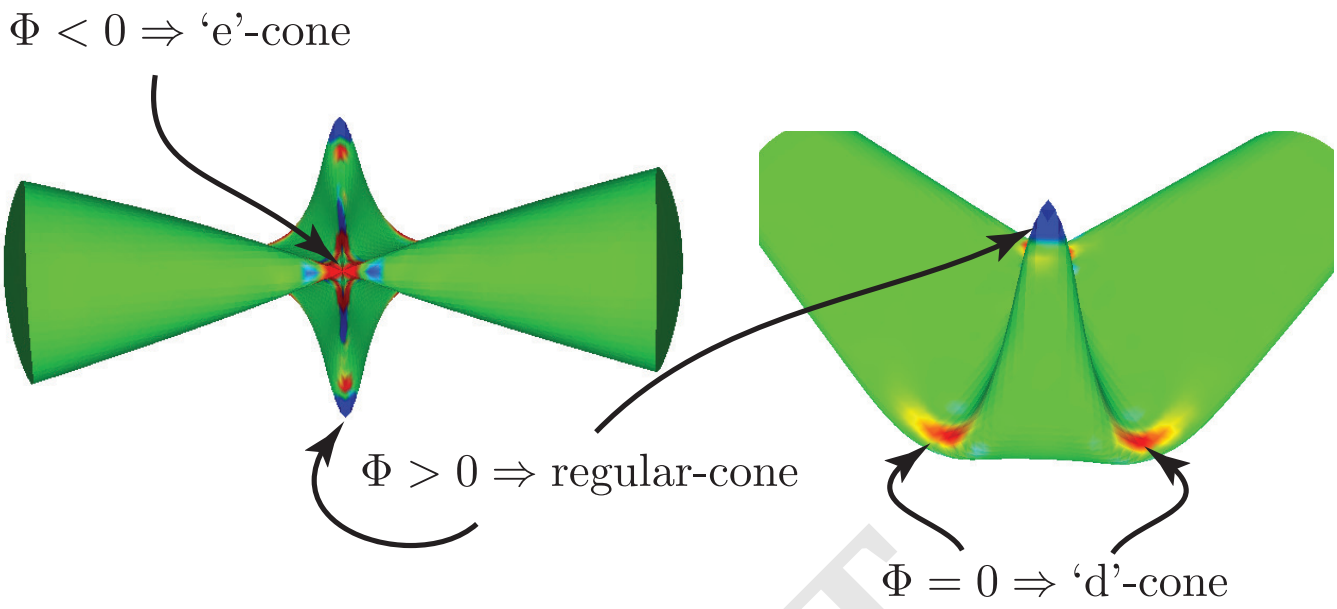

Fig. 9. Supplemental figure 1: The geometry of conical points in a Heineke-Mikulicz strictureplasty. Our prior work () showed that the shape is dominated by the 'e'-cone which forms by joining the two vertices of the initial enterotomy during the transverse closure. The regular-cones flank the suture line and as noted in the main text are typically though of as dog ears. By the Gauss-Bonnet theorem, since a strictureplasty only involves making a cut and re-orienting the cut via transverse closure, the overall topology of the deformed cylinder is preserved: $\Phi_{\text{'e'-cone}} + \Phi_{\text{regular-cone}} = 0$. Away from the suture line four flanking 'd'-cones appear.

DRAFT

1. Aly OE. A new direction in anastomotic research: should we redesign the 'angle of sorrow'? *Int J Colorectal Dis*, 33(2):159–162, 2018.
2. Halsted WS. Circular suture of the intestine – an experimental study. *Am J Med Sci*, 188:436–461, 1887.
3. Gajendran M, Bauer AJ, and Buchholz BM et al. Ileocecal anastomosis type significantly influences long-term functional status, quality of life, and healthcare utilization in postoperative crohn's disease patients independent of inflammation recurrence. *Am J Gastroenterol*, 113(4):576–583, 2018.
4. Yeo CJ, Matthews JB, and McFadden DW et al. *Shackelford's Surgery of the Alimentary Tract*. Saunders, 2012.
5. Hawley PR. Causes and prevention of colonic anastomotic breakdown. *Dis Colon Rectum*, 16(4):272–277, 1973.
6. Savin T, Kurpios NA, and Shyer AE et al. On the growth and form of the gut. *Nature*, 476:57–62, 2011.
7. Witten TA. Stress focusing in elastic sheets. *Rev Mod Phys*, 79:643–675, 2007.
8. Audoly B and Pomeau Y. *Elasticity and Geometry: From hair curls to the nonlinear response of shells*. Oxford University Press, 2010.
9. Pocivavsek L, Efrati E, and Lee KYC et al. Three-dimensional geometry of the heineke–mikulicz strictureplasty. *Inflamm Bowel Dis*, 19:704–711, 2013.
10. Efi Efrati, Luka Pocivavsek, Ruben Meza, Ka Yee C. Lee, and Thomas A. Witten. Confined disclinations: Exterior versus material constraints in developable thin elastic sheets. *Physical Review E*, 91 (2), feb 2015. . URL https://doi.org/10.1103%2Fphysreve.91.022404.
11. Tsamis A, Pocivavsek L, and Vorp DA. Elasticity and geometry: a computational model of the heineke–mikulicz strictureplasty. *Biomech Model Mechanobiol*, 13(6):1185–1198, 2014.
12. Hyoju SK, Klabbers RE, and Aaron M et al. Oral polyphosphate suppresses bacterial collagenase production and prevents anastomotic leak due to serratia marcescens and pseudomonas aeruginosa. *Ann Surg*, 267(6):1112–1118, 2018.
13. Shogan BD, Belogortseva N, and Luong PM et al. Collagen degradation and mmp9 activation by enterococcus faecalis contribute to intestinal anastomotic leak. *Sci Transl Med*, 7(286):286ra68, 2015.
14. Shakhsheer BA, Versten LA, and Luo JN et al. Morphine promotes colonization of anastomotic tissues with collagenase - producing enterococcus faecalis and causes leak. *J Gastrointest Surg*, 20: 1744–1751, 2016.
15. P Ciarletta, P Dario, F Tendic, and S Micera. Hyperelastic model of anisotropic fiber reinforcemens within intestinal walls for applications in medical robotics. *Int J Robotics Research*, 28(10): 1279–1288, 2009.
16. Ogden RW. *Nonlinear Continuum Mechanics and Modeling the Elasticity of Soft Biological Tissues with a Focus on Artery Walls. In: Holzapfel G., Ogden R. (eds) Biomechanics: Trends in Modeling and Simulation. Studies in Mechanobiology, Tissue Engineering and Biomaterials*, volume 20. Springer, 2017.
17. Y. Yoshiumra. On the mechanism of buckling of a circular cylindrical shell under axial compression. *echnical Memorandum 1390. National Advisory Committee for Aeronautics.*, July 1955.
18. P Saez, E Pena, M A Martinez, and E Kuhl. Computational modeling of hypertensive growth in the human carotid artery. *Comput Mech*, 53:1183–1196, 2014.
19. N J B Driessen, M A J Cox, C V C Bouten, and F P T Baaijens. Remodelling of the angular collagen fiber distribution in cardiovascular tissues. *Biomech Model Mechanobiol*, 7(2):93–103, 2008.
20. Ward MA, Pierre JF, and Leal RF et al. Insights into the pathogenesis of ulcerative colitis from a murine model of stasis-induced dysbiosis, colonic metaplasia, and genetic susceptibility. *Am J Physiol Gastrointest Liver Physiol*, 310:G973–G988, 2016.
21. Koch RG, Tsamis A, and D'Amore A et al. A custom image-based analysis tool for quantifying elastin and collagen micro-architecture in the wall of the human aorta from multi-photon microscopy. *J Biomech*, 47(5):935–943, 2014.
22. Zeng YJ, Qiao AK, and Yu JD et al. Collagen fiber angle in the submucosa of small intestine and its application in gastroenterology. *World J. Gastroenterol*, 9(4):804–807, 2003.
23. Annaidh AN, Bruyere K, and Destrade M et al. Characterization of the anisotropic mechanical properties of excised human skin. *J Mech Behav Biomed Mater*, 5(1):139–148, 2012.
24. Abaqus. *Abaqus User's Manual, Vs.6.18*. Dassault Systemes, Simulia Corporation,RI, 2018.
25. T C Gasser, R W Ogden, and G A Holzapfel. Hyperelastic modelling of arterial layers with distributed collagen fiber orientations. *J R Soc Interface*, 3(6):15–35, 2006.
26. N Nguyen, N Nath, L Deseri, E Tzeng, S S Velankar, and L Pocivavsek. Wrinkling instabilities for biologically relevant fiber-reinforced composite materials with a case study of neo-hookean/ogden–gasser–holzapfel bilayer. *Biomech Model Mechanobiol*, 19:2375–2395, 2020.